RSC Advances

ROYAL SOCIETY OF CHEMISTRY

www.rsc.org/advances

1   # Synthesis and Characterization of Flurbiprofen axetil-loaded

2   # Electrospun MgAl-LDHs/ poly(lactic-co-glycolic acid) Composite

3   # Nanofibers

4   Chunyu Yang, Tonghe Zhu, Jihu Wang, Sihao Chen[*], Wenyao Li[**]

5

6   **Abstract**

7   We have reported a facile method to fabricate drug-loaded hybrid nanofibers for drug sustained

8   release. In our work, a model drug FA was intercalated into the interlayers of layered double

9   hydroxides (LDHs) by ultraphonic intercalation. The particles were dispered into the PLGA

10   solution to form the electrospun hybrid nanofibers. The intercalation of FA into the LDHs

11   interlayers (MgAl-FA-LDHs) and the composite nanofibers were characterized via different

12   techniques. The results of XRD and FTIR indicate that FA molecules are intercalated into the

13   MgAl-LDHs interlayers. The formed composite nanofibers exhibt a uniform and smooth

14   morphology and the hydrophily didn't improve significantly. Importantly, the drug-loaded

15   MgAl-FA-LDHs/PLGA shows a sustained release profile which indicates the MgAl-LDHs can be

16   a candidate for drug sustained release.

17

18   **Keywords:** Electrospinning; Flurbiprofen axetil; Layered double hydroxides (LDHs);

19   Poly(lactic-co-glycolic acid); Intercalation; Drug delivery

20

21   **1. Introduction**

22   The flurbiprofen axetil (FA) is a kind of lipid microsphere non-steroidal anti-inflammatory

23   drug.[1-3] Pain on injection is an acknowledged adverse (AE) of propofol administration for the

24   induction of general anesthesia. Flurbiprofen axetil has been reported to reduce the pain of

25   injection.[4-6] However, results of published papers on the efficacy of flurbiprofen axetil in

26   managing pain on injection of propofol are inconsistent.

27   Layered double hydroxides (LDHs) are well known biocompatible inorganic materials that

28   have recently been used for the development of drug delivery and controlled release systems.[7-13]

29   LDHs, which are also known as anionic clay or hydrotalcite-like compounds, can be represented

30   by the general formula $[M_{1-x}^{2+}M_x^{3+}(OH)_2](A^{n-})_{x/n} \cdot mH_2O$, where M^{2+} and M^{3+} are di- and

*Corresponding author at: College of Chemistry and Chemical Engineering, Shanghai University of Engineering Science, Shanghai 201620, People's Republic of China.
Tel.: +86 21 67791239; fax: +86 21 67791239.
**Corresponding author:
  E-mail addresses: chensh@sues.edu.cn (S. Chen), liwenyao314@gmail.com (W. Li).

31 trivalent cations, respectively, and A^{n-} is the interlayer anion. LDH layers possess positive charges

32 because of the isomorphous substitution, which is balanced by interlayer hydrated anions. The

33 lamellar structure and anion exchange properties of LDHs enable some anionic drugs and

34 bio-molecules to be readily intercalated into their interlayer to form drug or bio-LDH nanohybrids.

35 Electrospinning, a technique producing ultrafine fibers with diameters ranging from tens of

36 nanometers to several microns, has attracted much attention due to its versatility and potential for

37 applications in the fields of tissue engineering[14-18] and pharmaceutical science.[19-23] Particularly,

38 electrospun nanofibers with remarkable features such as high porosity, high specific surface area,

39 good structure controllability and space grid structure make them well suited for drug delivery,

40 cell proliferation and tissue repair.[24,25] In our previous work, we have shown that flurbiprofen

41 axetil (FA) drug molecules were physically encapsulated within the polyvinylpyrrolidone (PVP),

42 followed by electrospinning the mixture solution of biopolymers and FA-loaded PVP to form a

43 composite drug incorporated nanofiber, which was proved to be able to significantly alleviate the

44 burst release of FA.[26,27]

45 In this work, we attempted to develop a facile approach to fabricating MgAl-LDHs -doped

46 PLGA nanofibers via electrospinning for drug encapsulation and release. A model drug FA was

47 first intercalated into the MgAl-LDHs interlayers via an ion-exchange intercalation method. Then

48 the FA-intercalated MgAl-LDHs particles were mixed with PLGA solution for subsequent

49 formation of electrospinning MgAl-FA-LDHs/PLGA composite nanofibers (**Scheme 1**).

50 Compared with other drug-loaded systems (such as hybrid drug-loaded system and coaxial

51 electrospinning drug-loaded system, etc.), this drug-loaded system could improve the burst release

52 phenomenon at the initial phase of drug release to some extent. The intercalation of FA into

53 MgAl-LDHs interlayers and the formation of MgAl-FA-LDHs/PLGA composite nanofibers were

54 characterized using different techniques. The release kinetics of FA from the composite

55 MgAl-FA-LDHs/PLGA nanofibers was investigated using UV-Vis spectroscopy and compared

56 with FA/MgAl-LDHs mixture, MgAl-FA-LDHs particles and FA/PLGA nanofibers.
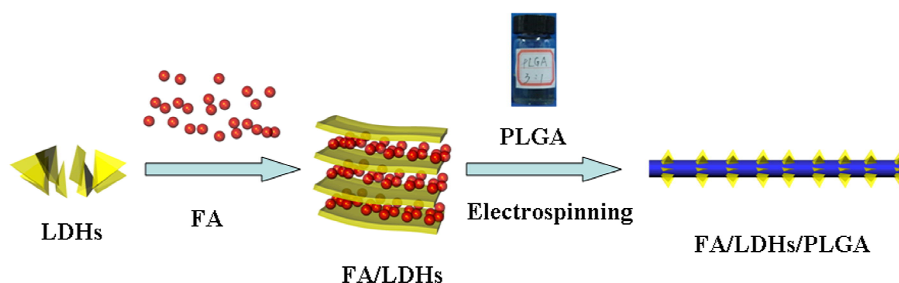
57

58 **Scheme 1.** Schematic illustration of the encapsulation of FA within LDHs-doped PLGA nanofibers.

59

60 ## 2. Experimental section

2.1 Materials

PLGA (M_W = 100 000 g/mol) with a lactic acid/glycolic acid ratio (molar ratio) of 50:50 and FA (purity > 99%) were purchased from Jinan Daigang Biotechnology Co., Ltd. (Shandong, China) and Shanghai Xinya Pharmaceutical Co., Ltd. (Shanghai, China), respectively. NO_3-LDHs was homemade and the particle size distribution ranged from 60 to 100 nm. Tetrahydrofuran (THF) and N, N-dimethylformamide (DMF) which are analytically pure (AR) were purchased from Sinopharm Chemical Reagent Co., Ltd. (Shanghai, China). All the other reagents used were of analytical grade and were used without further purification. The water used in the current study was purified.

2.2 Intercalation of FA into the interlayers of LDHs

An EtOH solution of FA (10 mL, 4 mg/mL) was added dropwise into a THF suspension of sieved NO_3-LDHs (10 mL, 3 mg/mL) and stirred (3000 r/min) for 30 min. Under nitrogen atmosphere, the 2 mol/L NaOH and 0.5mol/L Na_2CO_3 mixture was dropped into the above mixture to hold constant pH which equaled 10. The exchange process was stirred vigorously for 24 h at room temperature. The formed MgAl-FA-LDHs nanohybrid was separated by centrifugation (5000 rpm, for 5 min) and washed with EtOH three times to remove the excess free FA non-intercalated into the MgAl-LDHs interlayers. The FA concentration in the supernatant was analyzed using a 752N UV-Vis spectrophotometer (Jingke industrial co., LTD, Shanghai, China) at 254 nm using a standard FA concentration-absorbance calibration curve and the FA loading percentage was calculated by Eq. (1):

$$\text{FA intercalation percentage} = M_a / (M_a + M_0) \times 100\% \qquad (1)$$

Where M_a and M_0 stands for the mass of intercalated FA and the MgAl-LDHs carrier, respectively. Finally, the MgAl-FA-LDHs was lyophilized, ground down, and sieved to have a uniform size for subsequent electrospinning process. The drug intercalation percentage was optimized by changing the concentrations of FA and MgAl-LDHs, respectively.

2.3 Preparation of electrospinning MgAl-FA-LDHs/PLGA nanofibers

PLGA was dissolved in THF/DMF (v/v = 3:1) at an optimized concentration of 20 wt%. MgAl-FA-LDHs powder (1 wt% FA relative to PLGA) was then blended with PLGA solution for subsequent electrospinning. For comparison, a predetermined amount of MgAl-LDHs (5 wt% relative to PLGA) was added to PLGA solution and stirred for 1 h to get a homogeneous solution. The electrospinning nanofibers were prepared with an electrospinning equipment (SS-2534H Electrospinning Equipment, Beijing Ucalery Technology Co., Ltd., Beijing, China) using a stainless steel needle with an inner diameter of 0.6 mm. A voltage of 15 kV was applied to the collecting target by a high voltage power supply, the nanofibers were collected on a target drum placed 14 cm from the syringe tip and the roller rotation speed was 30 revolutions per minute, and

96 the electrospinning solution flow rate of 1.5 mL/h controlled by a syringe pump. The formed

97 electrospun fibrous mats were vacuum dried at room temperature for at least 2 d to remove the

98 residual organic solvent and moisture.

99 **2.4 Characterization**

100 The crystalline structure of the samples was analyzed by X-ray diffraction (XRD) on a

101 wide-angle analyzer (D/max-2500PC, Bruker) with a CuKα source ($\lambda = 0.154$ nm) operating at

102 100 mA and 40 kV. The diffraction patterns were collected from 5° to 80° (2θ) at a scanning rate

103 of 10°/min.

104 Fourier transform infrared spectroscopy (FTIR) was performed using a Nicolet FT-IR 370

105 spectrometer in a wavenumber range from 500 to 4000 cm^{-1} with a resolution of 2 cm^{-1} to confirm

106 the loading of FA into the MgAl-LDHs interlayers. The dried samples were mixed with KBr

107 crystals and pressed into pellets before measurements.

108 Morphologies of pure PLGA, FA/PLGA, MgAl-LDHs/PLGA, and MgAl-FA-LDHs/PLGA

109 were observed by a scanning electron microscope (SEM) (SU8010, Hitachi, Japan). The samples

110 were sprayed gold with a thickness about 10 nm before observation and the diameters of the fibers

111 were measured and statistics by a Image-Pro Plus software.

112 The hydrophobic or hydrophilic performance of the nanofiber membranes were measured by

113 a JC2000D2A water contact angle tester (Zhongchen digital technic apparatus co., ltd, Shanghai,

114 China). The samples were cut into 20 mm×20 mm and attached to the glass slides, and one droplet

115 of distilled water about 2 µl was dropped onto the random area of each membrane at room

116 temperature and humidity. Each sample needs to be measured five times.

117 **2.5 In vitro drug release**

118 The release of FA from MgAl-FA-LDHs particle, FA/PLGA and MgAl-FA-LDHs/PLGA was

119 determined by the absorbance of FA in phosphate-buffered saline (PBS) at 254 nm using a 752N

120 UV-Vis spectrophotometer (Jingke industrial co., Ltd, Shanghai, China). For the MgAl-FA-LDHs

121 particles, 20 mg was put into a dialysis tube containing 5 ml PBS (pH=7.4). Then the dialysis tube

122 was placed into a conical flask with 45 ml PBS. While for nanofiber membranes, a certain amount

123 of FA/PLGA and MgAl-FA-LDHs/PLGA nanofiber membranes was weighed to ensure that the FA

124 in the membranes had the approximate weight with the FA in the MgAl-FA-LDHs particles and

125 added into the different conical flasks containing 50 ml PBS. All the conical flasks were numbered

126 and incubated in a incubator shaker at 37 □ with a vibrating speed of 100 rpm. The experiment

127 was done in triplicate. At scheduled time intervals, 3 ml PBS was taken and other 3 ml fresh PBS

128 was added to ensure the solution environment rough balance.

129

130 **3. Results and discussion**

131   **3.1 Intercalation of MgAl-LDHs with FA**

132
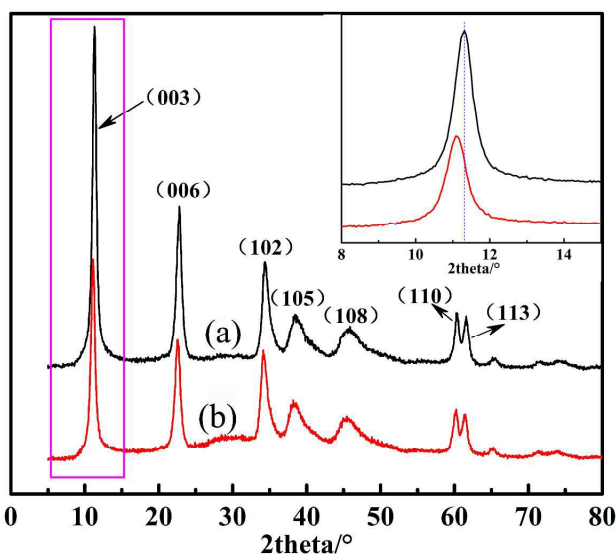
133   **Fig.1** XRD patterns of (**a**) pristine MgAl-LDHs and (**b**) MgAl-FA-LDHs.

134   The powder XRD patterns of the pristine MgAl-LDHs and MgAl-FA-LDHs are shown in **Fig.**

135   **1**. The pristine MgAl-LDHs and the MgAl-LDHs intercalation with FA almost have the same

136   sharp absorption peak at (003), (006), (102), (110) and (113) planes and broad asymmetric peaks

137   at (105) and (108) planes which are the characteristic peaks of MgAl-LDHs.[28] The intercalation of

138   FA made the peak at (003) plane generate "blue shift" about 0.4 ° (2θ from 11.33° to 10.98°) and

139   the intensity of the peak which we could see in the top right-hand corner of the XRD patterns

140   became a little weak. The calculation of the layer spacing via Bragg equation found that the layer

141   spacing of MgAl-LDHs was 0.78 nm, while for the MgAl-LDHs intercalated with FA, the layer

142   spacing was 0.81nm. The increase of the MgAl-LDHs indicated that FA was intercalated into the

143   interlayer of MgAl-LDHs.

144
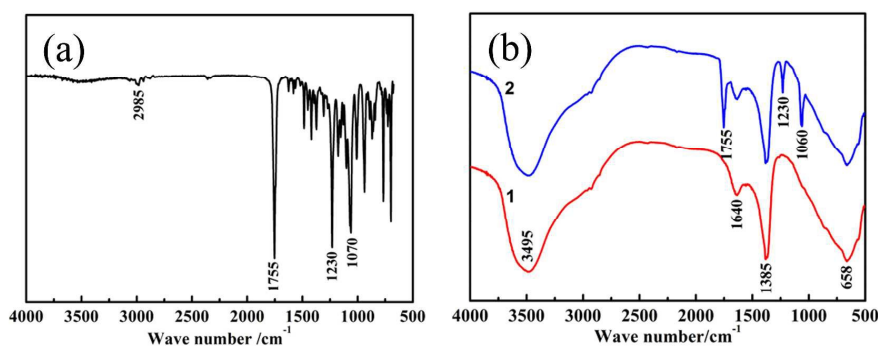
145   **Fig. 2** FTIR spectra of free FA (**a**), and MgAl-LDHs before (Curve **1**) and after (Curve **2**) FA loading (**b**).

146   The successful intercalation of FA into the MgAl-LDHs was also qualitatively confirmed by

147   FTIR spectroscopy (Fig. 2). In Fig. 2(**a**), the typical absorption bands at 1755, 1230 and 1070 cm^{-1}

148   are due to the carbonyl group, the stretching vibration of C=C group and the stretching vibration

149   of C–C bond of FA, respectively. The weak peak near 3000 cm^{-1} is attributed to the absorption

150   band of the C–H. In Fig. 2(**b**) (Curve **1**), the broad absorption peak near 3500 cm^{-1} is due to the

151   stretching vibration of O–H groups of both the hydroxide layer and interlayer bonding water. The

152   weak band at 1640 cm^{-1} is ascribed to the C=O bond of CO_3^{2-}. The strong absorption band at 1385

153   cm^{-1} is caused by the asymmetric stretching vibration C–O of the CO_3^{2-}, compared with the

154   wavenumber of free state CO_3^{2-} at 1415 cm^{-1}, this peak obviously shifts to low wavenumbers ("red

155   shift"), which indicates CO_3^{2-} inserted between layers are not free state any more but have strong

156   hydrogen bonds with the interlaminar water molecules. In the low-frequency region, the bands at

157   658 cm^{-1} is considered to the lattice vibration modes due to M–O and O–M–O vibrations.[29,30] In

158   the MgAl-FA-LDHs (Curve **2**), the absorption band at 1750 cm^{-1} is assigned to the stretching

159   vibration of the carbonyl group, while the weak peaks at 1230 and 1060 cm^{-1} correspond to the

160   stretching vibrations of C=C and C–C, respectively. Upon comparing FTIR spectra of the

161   intercalation MgAl-FA-LDHs with FA itself, it is clear that FA is intercalated MgAl-LDHs

162   successfully and the struture of drug molecules is not changed.
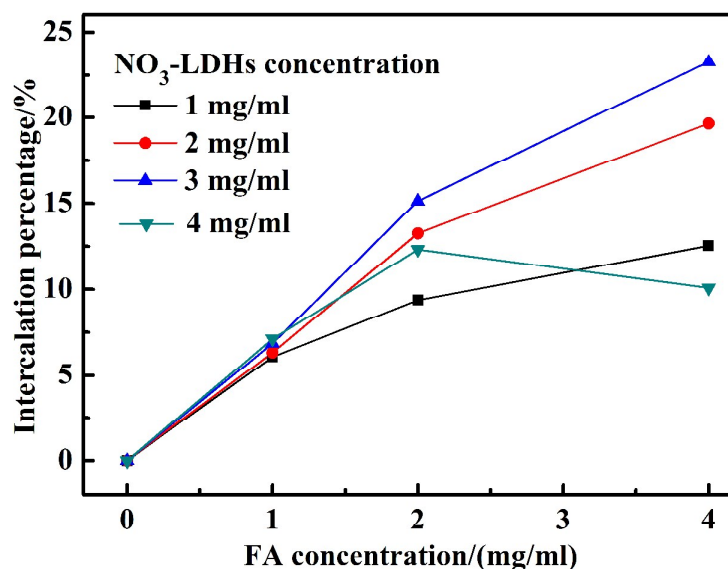
163

164   **Fig. 3** The FA intercalation percentage as a function of FA concentration under different NO$_3$-LDHs

165   concentrations.

166   The intercalation percentage of FA into MgAl-LDHs was optimized by regulating the

167   respective concentration of NO$_3$-LDHs and FA at the same experimental conditions. Fig. 3 shows

168   the profile of the FA intercalation percentage as a function of FA concentration under different

169   NO$_3$-LDHs concentrations. It is clear that the FA intercalation percentage increases with the

170   increase of FA concentration and as the NO$_3$-LDHs concentration increases, the FA intercalation

171   percentage increases first then increases slowly, even when the concentration of NO$_3$-LDHs is 4

172   mg/ml, the FA intercalation percentage appears increase first then decrease. This could be ascribed

173   to the aggregation of NO_3-LDHs at high concentration, which limited the intercalation of FA

174   molecules. Therefore, the optimized FA intercalation percentage is 23.26% at the optimized

175   concentration of FA (4 mg/mL) and NO_3-LDHs (3 mg/mL).

176   **3.2 Fabrication of electrospinning FA/MgAl-LDHs/PLGA nanofibers**

177   The obtained FA/MgAl-LDHs particles with optimized FA intercalation percentage were then

178   doped with PLGA solution via electrospinning to fabricate MgAl-FA-LDHs/PLGA composite

179   nanofibers (**Scheme 1**). As a reference for comparison, pure PLGA nanofibers, FA-doped PLGA

180   nanofibers and MgAl-LDHs-doped PLGA nanofibers without FA were also prepared in the same

181   condition. The surface morphology of the PLGA, FA/PLGA, MgAl-LDHs/PLGA,

182   MgAl-FA-LDHs/PLGA nanofibers were observed by SEM (**Fig. 4**). As shown in Fig. 4, PLGA

183   (**Fig. 4a**) and FA/PLGA (**Fig. 4b**) nanofibers exhibited uniform and smooth morphology, which

184   indicated good electrospinnability of PLGA.[31-33] While the incorporation of MgAl-LDHs and

185   MgAl-FA-LDHs altered the uniform morphology of PLGA nanofibers and some "beaded" fibers

186   formed (**Fig. 4c and Fig. 4d**). The diameters of electrospun PLGA, FA/PLGA,

187   MgAl-LDHs/PLGA, FA/MgAl-LDHs/PLGA nanofibers were estimated to be 906 ± 317 nm, 992

188   ± 205 nm, 1014 ± 414 nm and 1028 ± 210 nm, respectively. The larger diameters of FA/PLGA,

189   MgAl-LDHs/PLGA and FA/MgAl-LDHs/PLGA composite nanofibers than that of pure PLGA

190   nanofibers are presumably attributed to the large increase of the conductivity of the solution,

191   which causes the increase of the flow rate of the solution, thus making the diameter of the

192   nanofibers increase. Additionally, the excess additives make the increase of the viscosity of the

193   solution which can drastically increase the viscous stress and in consequence the fiber diameter

194   increases.
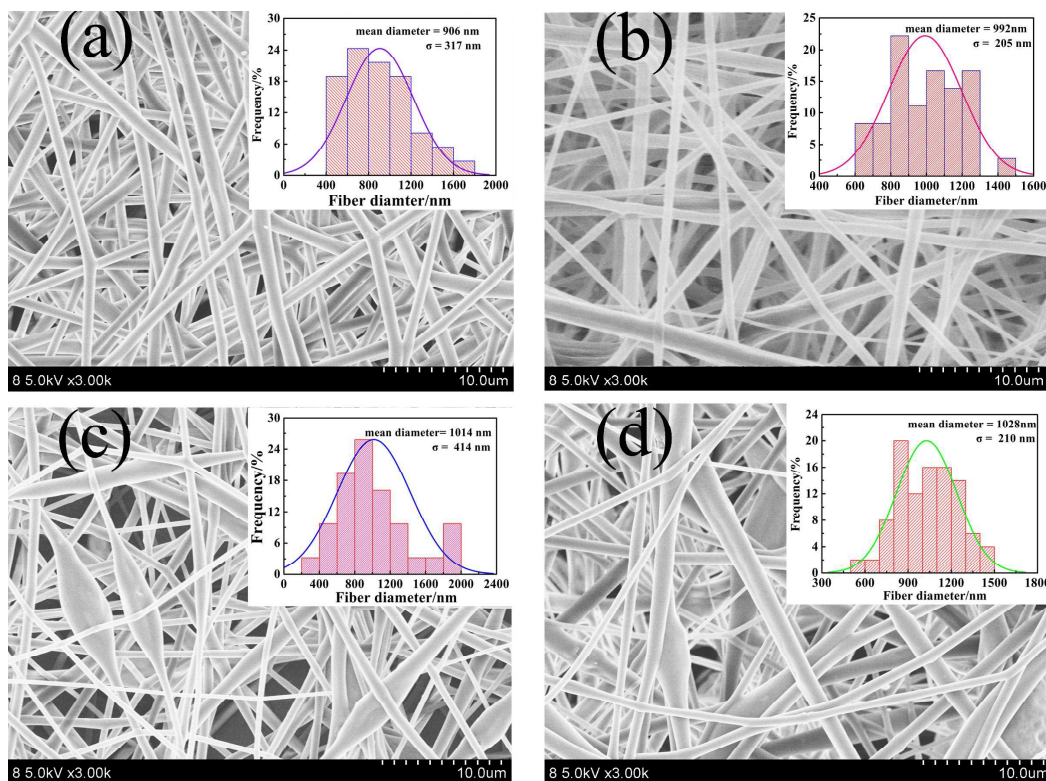
Fig. 4 SEM micrographs and diameter distribution histograms of electrospun PLGA fibers, (**a**) pure PLGA fibers, (**b**) FA/PLGA composite fibers (4 wt% FA relative to PLGA), (**c**) MgAl-LDHs/PLGA composite fibers (5 wt% MgAl-LDHs relative to PLGA)and (**d**) MgAl-FA-LDHs/PLGA composite fibers(5 wt% MgAl-FA-LDHs relative to PLGA).
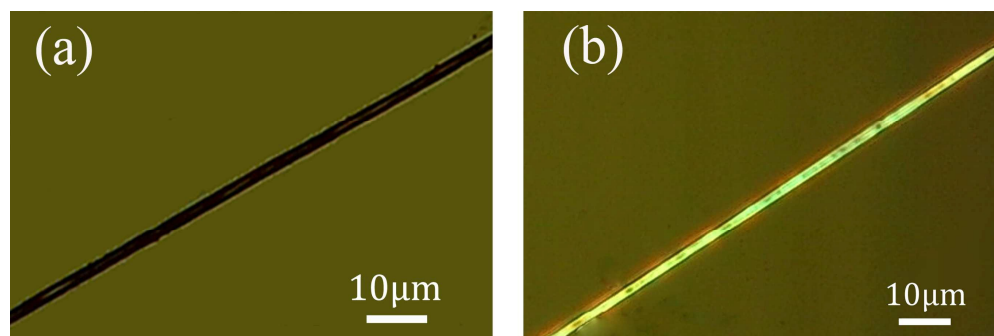
Fig. 5 Metallurgical microscope images of (**a**) pure PLGA and (**b**) MgAl-LDHs/PLGA fibers under the polarized light in dark field

In order to confirm the exsitence of MgAl-LDHs in the composite nanofibers, pure PLGA and MgAl-LDHs/PLGA nanofibers were observed under metallurgical microscope under the polarized light in dark field (**Fig. 5**). It is clear that the pure PLGA nanofibers (**Fig. 5a**) under metallurgical microscope present dark because PLGA itself is opaque and it presents original colour. While for MgAl-LDHs/PLGA naofibers (**Fig. 5b**), the MgAl-LDHs is crystal and appears bright under the polarized light in dark field, which is consistent with the reported literature.[34]
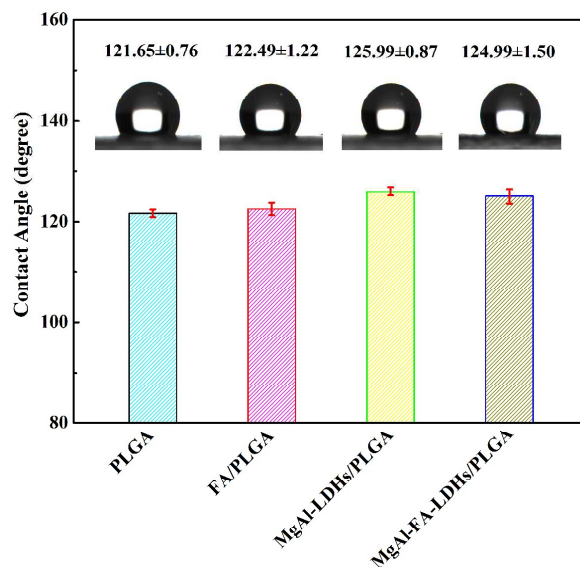
209

210 **Fig. 6** Water contact angle of PLGA, FA/PLGA, MgAl-LDHs/PLGA and MgAl-FA-LDHs/PLGA nanofibers. Data
211 are shown as mean ± SD (n = 5)

212   Surface hydrophilicity is an important parameter for electrospun nanofibers to be used in
213 biomedical applications. Fig. 6 shows the water contact angle variations of the electrospun PLGA,
214 FA/PLGA, MgAl-LDHs/PLGA and FA/MgAl-LDHs/PLGA nanofibers. It can be seen that the
215 water contact angle of the pure PLGA nanofibers was 121.65 ± 0.76 °, indicating PLGA is
216 hydrophobic.[35,36] While the incorporation of FA, MgAl-LDHs, FA/MgAl-LDHs does not seem to
217 significantly change the hydrophilicity of the nanofiber membrances, this is likely due to the
218 diameter of the fibers does not alter largely.

219 **3.3 Release of FA from MgAl-FA-LDHs/PLGA composite nanofibers**

220   Drug release profiles for FA/MgAl-LDHs mixture, MgAl-FA-LDHs, FA/PLGA nanofibers
221 and MgAl-FA-LDHs/PLGA nanofibers are presented in Fig. 7. For FA/MgAl-LDHs mixture (**Fig.
222 7a**), the drug release rate was very rapid and the drug release cycle was very short, about 2 h.
223 Because the method of physical hybrid only made FA molecules adsorb on the MgAl-LDHs and
224 the interaction was very weak, FA molecules were very easy to be separated from MgAl-LDHs in
225 the process of drug release. Additionally, it is clear that both MgAl-FA-LDHs and FA/PLGA
226 nanofibers (**Fig. 7b**) shows an obvious initial burst release in the inital 24 h. Within the first 24 h,
227 approximate 70% of the drug was released and only about 10% was released at the following 4
228 days with a relatively slow speed (totally released < 80% in 5 days). By contrast, the FA release
229 from MgAl-FA-LDHs/PLGA nanofibers (**Fig. 7b**) needs to go through two processes: the FA
230 molecules dissociate from the interlays of MgAl-LDHs and the free FA molecules diffuse from the
231 PLGA fiber mat. Therefore, about 24% of the FA was released in the initial 24 h and the release
232 was very slow at the following two days which tended towards stability after day 3. So, only
233 39.19 % of the FA was released in 5 days.
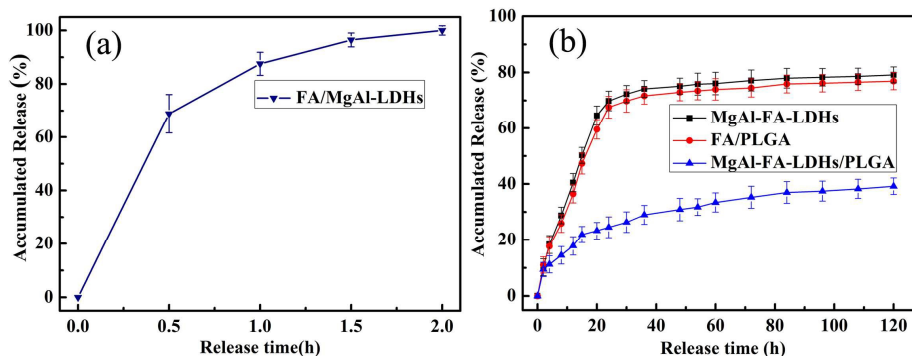
Fig. 7 In vitro release of FA from (**a**) FA/MgAl-LDHs mixture and (**b**) MgAl-FA-LDHs, FA/PLGA nanofibers and MgAl-FA-LDHs/ PLGA nanofibers with similar mass of FA.

The rapid release of FA from MgAl-FA-LDHs (**Fig. 7b**) could be due to the fact that the physical interaction between the FA molecule and MgAl-LDHs is weak hydrogen bonding. While, for FA/PLGA nanofibers (**Fig. 7b**), the rapid release of FA from the composite nanofibers could be ascribed to on the one hand the FA which is not coated on the surface of the fibers and on the other hand the weak interaction between FA and PLGA. Therefore, for both MgAl-FA-LDHs and FA/PLGA nanofibers, the phenomenon of burst release appears at the initial phase. However, for MgAl-FA-LDHs/PLGA nanofibers drug carrier, the intercalated FA drug molecules should first be dissociated from the interlays of MgAl-LDHs to the PLGA matrix, and then the free drug molecules diffuse from the solid PLGA matrix to the PBS. With the concentration of FA in the PBS increase, the diffusion impetus decreases gradually and tends to stability at last, thereby gaining a sustained release profile. The simliar burst release phenomenon occurs in MgAl-FA-LDHs/PLGA nanofibers drug carrier in the initial 15 h, it could be due to the strong electrostatic interactions that makes partial FA molecules dissociate from MgAl-LDHs during the electrospinning process and the partial MgAl-FA-LDHs uncoated by PLGA matrix. This indicates that the drugs intercalated in the MgAl-FA-LDHs/PLGA nanofibers are more difficult to release than those in the FA/PLGA nanofibers and it can be concluded that MgAl-LDHs are more suitable as a controlled-release host.

4. Conclusions

In summary, FA was successfully intercalated into the MgAl-LDHs interlayers by ion-exchange method and the MgAl-FA-LDHs/PLGA nanofibers obtained via a hybrid electrospinning. The incorporation of drug-intercalated MgAl-LDHs not only significantly reduced the burst release of the drug, but also appreciably extended the released time of the drug. For MgAl-FA-LDHs/PLGA nanofibers drug system, the intercalated FA drug molecules should first be dissociated from the interlays of MgAl-LDHs to the PLGA matrix, and then the free drug

262   molecules diffuse from the solid PLGA matrix to the PBS, which is proven to be the an efficient

263   strategy to slow down the release rate of FA.

264

265   **Acknowledgements**

270

271   **References**

272   1 J. Q. Shen, L. Gan, C. L. Zhu, X. X. Zhang, Y. Dong, M. Jiang, J. B. Zhu and Y. Gan, *Int. J. Pharm.*, 2011, 412,

273   115–122.

274   2 Y. J. Xu, Z. M. Tan, J. W. Chen, F. F. Lou and W. Chen, *Ca. J. Anesth.*, 2008, 55(7), 414–422.

275   3 X. Lin, R. Q. Zhang, J. C. Xing, X. C. Gao, P. Chang and W. Z. Li, *Int J Clin Exp Med.*, 2014, 7(12), 4887–4896.

276   4 L. L. Zhang, J. Zhu, L. Xu, X. L. Zhang, H. Y. Wang, Z. H. Luo, Y. M. Zhao, Y. Yu, Y. Zhang, H. W. Shi and H.

277   G. Bao, *Med. Sci. Monitor*, 2014, 06(20), 995–1002.

278   5 Y. Fujii, Y. Shiga, *Clin Ther.*, 2005, 27(5), 588–593.

279   6 Y. Fujii,and M. Itakura, *Clin Ther.*, 2008, 30, 280–286.

280   7 X. Bi, H. Zhang and L. G. Dou, *Pharmaceutics*, 2014, 6, 298–332.

281   8 K. Zhang , Z. P. Xu , J. Lu , Z. Y. Tang , H. J. Zhao , D. A. Good and M. Q. Wei, *Int. J. Mol. Sci.*, 2014, 15,

282   7409–7428.

283   9 V. Rives , M. D. Arco, C. Martín, *J. Control. Release*, 2013, 169, 28–39.

284   10 F. Barahuie, M. Z. Hussein , S. Fakurazi and Z. Zainal, *Int. J. Mol. Sci.*, 2014, 15, 7750–7786.

285   11 Z. Gu, A. C. Thomas, Z. P. Xu, J. H. Campbell and G. Q. Lu, *Chem. Mater.*, 2008, 20, 3715–3722.

286   12 J. H. Choy, J. S. Jung, J. M. Oh, M. Park, J. Y. Jeong , Y. K. Kang, O. J. Han, *Biomaterials*, 2004, 25,

287   3059–3064.

288   13 B. X. Li, J. He, D. G. Evans, X. Duan, *Appl. Clay Sci.*, 2004, 27, 199–207.

289   14 J. Stitzel, J. Liu, S. J. Lee, M. Komura, J. Berry, S. Soker, G Lim, M. Van Dyke, R Czerw, J. J. Yoo and A. Atala,

290   *Biomaterials*, 2006, 27(7), 1088–1094.

291   15 G. Sui, X. Yang, F. Mei, X. Hu, G. Chen, X. Deng, S. Ryu, *J. Biomed. Mater. Res. A*, 2007, 82(2), 445–454.

292   16 E. I. Paşcu, J. Stokes, G. B. McGuinness, *Mater. Sci. Eng. C Mater.*, 2013, 33, 4905–4916.

293   17 E. Schnell, K. Klinkhammer, S. Balzer, G. Brook, D. Klee, P. Dalton, J. Mey, *Biomaterials*, 2007, 28(19),

294   3012–3025.

295   18 X. He, L. Cheng, X. M. Zhang, Q. Xiao, W. Zhang, C. H. Lu, *Carbohyd. Polym.*, 2015, 115, 485–493.

296   19 H. Jiang, Y. Hu, P. Zhao, Y. Li, K. Zhu, *J. Biomed. Mater. Res. B*, 2006, 79(1), 50–57.

297   20 H. Jiang, Y. Hu, Y. Li, P. Zhao, K. Zhu, W. Chen, *J. Control. Release* , 2005, 108(2-3), 237–243.

298   21 N. Bolgen, I. Vargel, P. Korkusuz, Y. Z. Menceloglu, E. Piskin, *J. Biomed. Mater. Res. B*, 2007, 81(2), 530–543.

299   22 J. Xie, C. H. Wang, *Pharm. Res.*, 2006, 23(8), 1817–1826.

300   23 T. Potrcˇ, S. Baumgartner, R. Roškar, O. Planinšek, Z. Lavricˇ, J. Kristl, P. Kocbek, *Eur. J. of Pharm. Sci.*, 2015,

301   75, 101–113.

302   24 R.A. Thakura, C.A. Florekb, J. Kohnb, B.B. Michniaka, *Int. J. Pharm.*, 2008, 36, 87–93.

303   25 G. Kim, W. D. Kim, *J. Biomed. Mater. Res. B*, 2007, 81(1),104–110.

304   26 T. H. Zhu, C. Y. Yang, S. H. Chen, W. Y. Li, J. Z. Lou, J. H. Wang, *Mater. Lett.*, 2015, 150, 52–54.

305   27 T. H. Zhu, S. H. Chen, W. Y. Li, J. Z. Lou, J. H. Wang, *J. Appl. Polym. Sci.*, 2015, 132(22).

306   28 S. Kannan, and C.S. Swamy, *J. Mater. Sci.*, 1992, 11, 1585-1587.

307   29 J. T. Kloprogge and R. L. Frost, *J. Solid State Chem.*, 1999, 146, 506–515.

308   30 S. Aisawa, S. Takahashi, W. Oggasawara, Y. Umetsu, E. Narita, *J. Solid State Chem.*, 2001, 162, 52–62.

309   31 R. L. Qi, X. Y. Cao, M. W. Shen, R. Guo, J. Y. Yu, X. Y. Shi, *J. Biomater. Sci.-Polym. E.*, 2012, 1, 299–313.

310   32 F. J. Liu, R. Guo, M. W. Shen, X. Y. Cao, X. M. Mo, S. Y. Wang, *Soft Mater.*, 2010, 8, 239–253.

311   33 F. J. Liu, R. Guo, M. W. Shen, S. G. Wang, X. Y. Shi, *Macromol. Mater. Eng.*, 2009, 294, 666–672.

312   34 E. M. Seftel, E. Popovici, E. Beyers, M. Mertens, H. Y. Zhu, E. F. Vansant, and P. Cool, *J. Nanosci.*

313   *Nanotechno.*, 2010, 10, 1–7.

314   35 K. Nasouri, H. Bahrambeygi, A. Rabbi, A. M. Shoushtari, A. Kaflou, *J. Appl. Polym. Sci.*, 2012, 126(1),

315   127–135.

316   36 F. Fredenberg, M. Wahlgren, M. Reslow, A. Axelsson, *Int. J. Pharm.*, 2011, 415(1-2), 34–52.